PCCP

RSC Publishing

PAPER

View Article Online
View Journal | View Issue

Cite this: *Phys. Chem. Chem. Phys.*, 2013, **15**, 3725

Quantum chemical investigation of epoxide and ether groups in graphene oxide and their vibrational spectra†

Alister J. Page,[a] Chien-Pin Chou,[b] Buu Q. Pham,[c] Henryk A. Witek,[b] Stephan Irle*[d] and Keiji Morokuma*[ae]

Received 9th January 2013,
Accepted 16th January 2013

DOI: 10.1039/c3cp00094j

www.rsc.org/pccp

We present a detailed analysis of the factors influencing the formation of epoxide and ether groups in graphene nanoflakes using conventional density functional theory (DFT), the density-functional tight-binding (DFTB) method, π-Hückel theory, and graph theoretical invariants. The relative thermodynamic stability associated with the chemisorption of oxygen atoms at various positions on hexagonal graphene flakes (HGFs) of D_{6h}-symmetry is determined by two factors – *viz.* the disruption of the π-conjugation of the HGF and the geometrical deformation of the HGF structure. The thermodynamically most stable structure is achieved when the former factor is minimized, and the latter factor is simultaneously maximized. Infrared (IR) spectra computed using DFT and DFTB reveal a close correlation between the relative thermodynamic stabilities of the oxidized HGF structures and their IR spectral activities. The most stable oxidized structures exhibit significant IR activity between 600 and 1800 cm^{-1}, whereas less stable oxidized structures exhibit little to no activity in this region. In contrast, Raman spectra are found to be less informative in this respect.

Introduction

Graphene and graphene oxide (GO) are currently at the forefront of modern materials science and technology. Yet it was over a century ago, in 1859, that Benjamin Brodie isolated GO for the first time *via* the exfoliation of graphite oxide. The popularity of graphene and GO today stems from their outstanding physicochemical properties,[1,2] which make their application in nanoscale electronic and optical devices a potential reality. Structural models of GO have been reviewed on several recent occasions (see ref. 2–4 and references therein). Proposed GO structures and their dynamic and chemical behavior remain controversial. Perhaps the most popular structural proposal is that reported by Lerf and Klinowski *et al.*,[5,6] which assumes epoxides and alcohols to be the main features in the graphene basal plane, leaving the carbon σ-bond network intact. Conversely, the GO structure proposed by Dékány *et al.*[7] is dominated by ether and keto functional groups in the GO basal plane, assuming partial damage to the carbon σ-bond network. Recent experiments[8,9] suggest that oxidation results in both ether and epoxy groups in the GO basal plane, with the ratio of epoxy and ether groups being dependent on the extent of functionalization. Molecular dynamics simulations suggest that epoxide groups are able to migrate on the surface even at 300 K,[10] while other investigations point to a 'kinetically constrained' GO structure.[11,12] Oxidative linear unzipping of graphenes has been deemed possible,[13–15] but could not directly be confirmed in quantum chemical molecular dynamics simulations.[10]

One of the original questions regarding the distribution of GO functional groups following the initial non-stoichiometric, amorphous structures proposed by Lerf and Klinowski *et al.*[5,6] pertains to the distribution of functional groups. Do functional groups distribute themselves so that the area of uninterrupted

[a] *Fukui Institute for Fundamental Chemistry, Kyoto University, Kyoto 606-8103, Japan. E-mail: keiji.morokuma@emory.edu*
[b] *Department of Applied Chemistry and Institute of Molecular Science, National Chiao Tung University, Hsinchu 30010, Taiwan*
[c] *Institute for Computational Science and Technology, Vietnam National University, Ho Chi Minh City, Vietnam*
[d] *Department of Chemistry, Graduate School of Science, Nagoya University, Nagoya 464-8602, Japan. E-mail: sirle@chem.nagoya-u.ac.jp*
[e] *Cherry L. Emerson Centre for Scientific Computation and Department of Chemistry, Emory University, Atlanta, GA 30322, USA*

† Electronic supplementary information (ESI) available: Comparison of DFT/DFTB IR spectra and optimized geometries for HGF **1**; full lists of computed Kekulé structures *K* and Clar covers *C* for HGFs **1–11** and their graphical representations; comparison between Kekulé/Clar aromaticities and DFTB energies for HGFs **1–11**. See DOI: 10.1039/c3cp00094j

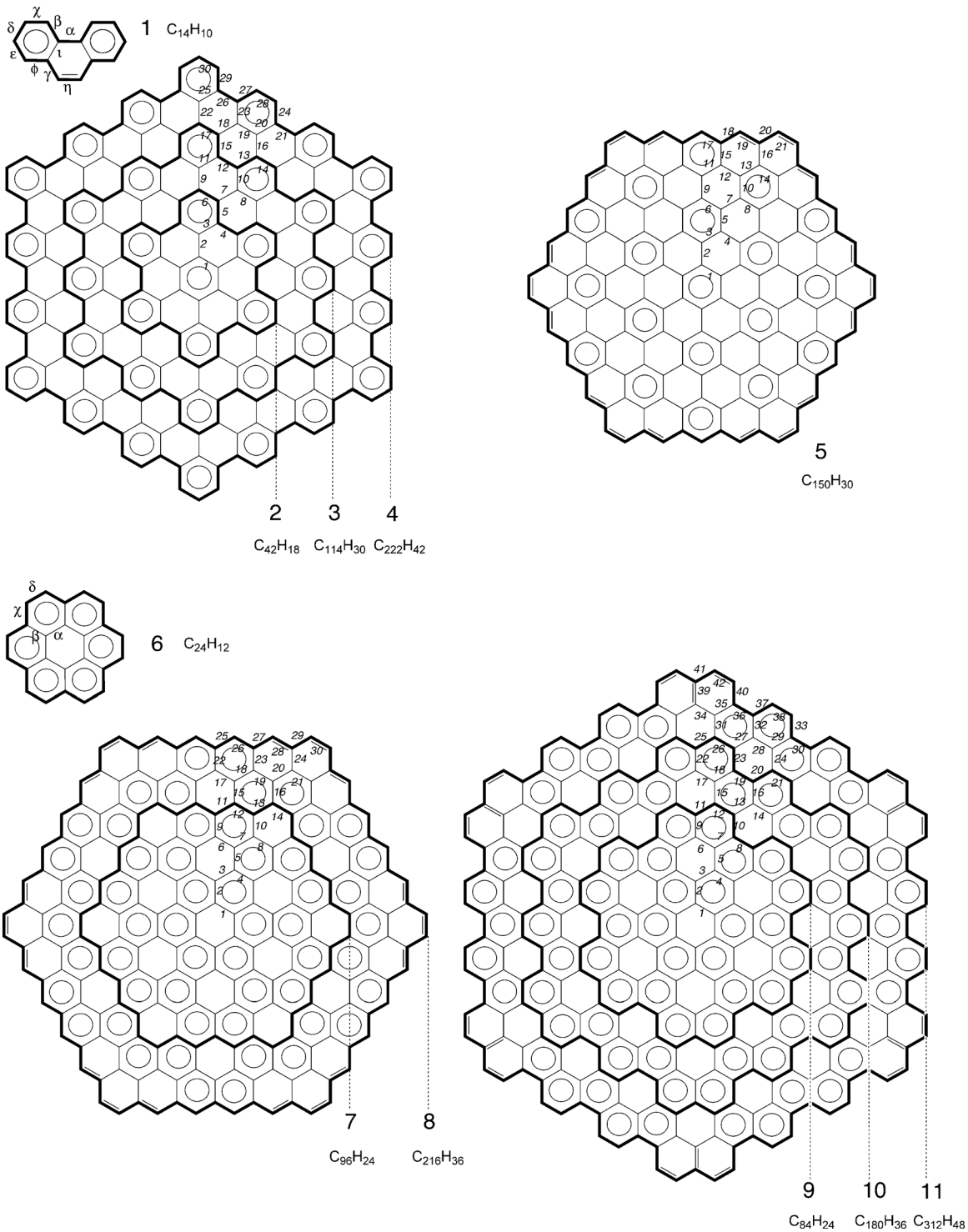

Fig. 1 Definition of nomenclature and stoichiometries for phenanthrene (**1**) and coronene (**6**) model systems and D_{6h} HGF structures **2–5** and **7–11**. Isolated and resonant π-electron Clar-sextet patterns are also depicted for each structure. For clarity, the isolated and resonant Clar-sextet pattern of only the largest member of each series is shown; edge hydrogen atoms are not depicted.

π-conjugated regions is maximized? As Dreyer *et al.*[3] note, the answer to this question underpins the chemical reactivity and electronic structure of GO. Several recent experiments (see ref. 4 and references therein) point to the existence of sp^2 'islands' of diameters between 2 and 3 nm in GO. Liu *et al.*[16] have also shown that amorphous GO models prefer a degree of short-range order. This question is important, since the applicability of graphenes – at least in the context of nanoelectronics – is determined primarily by their band gap, which is controlled in turn by the 'tunability' of their $sp^2 : sp^3$ carbon ratios.[4]

A detailed understanding of the factors governing competing oxidations in different regions of the graphene basal plane is therefore warranted, but has not yet been reported in the literature (despite an already rich theoretical literature concerning GO structure, see ref. 11 and references therein).

In this work we present a detailed study of the bonding of epoxide functional groups in the basal plane of D_{6h} hexagonal graphene flakes (HGFs) with both armchair and zigzag edges of increasing size (see Fig. 1). The bearing of the π-structure of the HGF on the epoxidation energetics will also be addressed, both from quantum chemical and graph theoretical points of view. This analysis will be presented in terms of phenanthrene and coronene archetypal HGFs (structures **1** and **6**, Fig. 1). Finally, we will show that the relative energetics of these GO flakes is commensurate with trends in their infrared (IR) spectra – *i.e.*, that IR spectral signatures are convenient indicators of these bonding trends. This in itself reflects experimental trends in the structural evolution during the thermal reduction of GO.[17,18] We will show, however, that Raman spectroscopy is less informative for discriminating these bonding trends in GO.

Computational details

Quantum chemical calculations

Density functional theory (DFT) and density functional tight-binding (DFTB) methods were employed to investigate the epoxidation of HGFs **1–11** (Fig. 1). The structure and IR spectra of the HGFs **2–5** and **7–11** and their oxides were considered only at the DFTB level. For DFT, the B3LYP functional,[19,20] as implemented in the G09 program,[21] was employed in conjunction with the 6-31G(d) split-valence basis set. The performance of this method has previously been validated in the context of GO.[14] Both the self-consistent charge DFTB (denoted simply DFTB for brevity) method[22] and the spin-polarized variant thereof (SDFTB)[23] were also employed. Self-consistency with respect to atomic charge fluctuations is essential for an accurate description of systems involving partial charge-transfer between atomic centers. Similarly, the inclusion of spin-polarization was required to investigate the energetics of oxidation resulting in both singlet and triplet HGF oxides. To assist in the convergence in the iterative solution of the DFTB/SDFTB equations, a low electronic temperature (T_e) of 100 K was imposed in both cases. The effect of such an inclusion is anticipated to be negligible on structural and spectral features of these species. For DFTB/SDFTB calculations of geometries and energies, the C/O/H parameters included in the mio-0-1 parameter set[22] were employed. For the computation of IR/Raman spectra using DFTB, C/O/H parameters[24] developed specifically for this purpose were employed in structure re-optimizations and second-order analytical geometrical derivative calculations, as well as for the calculation of IR and Raman intensities. The performance of DFTB in the context of IR/Raman spectroscopy has been demonstrated on a number of previous occasions;[25–28] in particular, spectroscopic trends obtained using DFTB have been shown to be the same as those using DFT. The same may be said regarding energetic trends for systems both physically related[29] and unrelated[30] to GO. All DFTB and SDFTB optimizations were performed using the G09 program,[21] with DFTB/SDFTB energies and gradients being computed externally.

We consider here GO structures (denoted by the suffix o) consisting of HGFs **1–11** with a single oxygen atom added above the midpoint of each symmetrically distinct C–C bond (these bonds are numbered in Fig. 1 for each HGF). The geometry of each isomer was then optimized, and the IR and Raman spectra were subsequently calculated.

Analysis of benzenoid Clar covers

In order to analyze local reactivity in a graphene nanoflake, we need to understand its π-electronic structure, in the sense first formulated by Schleyer and co-workers in 2003.[31] In this work, instead of performing nuclear independent chemical shift calculations, we resort to graph theoretical invariants in order to be able to deal with the largest HGF systems.

An arbitrary polyaromatic hydrocarbon (PAH) structure, such as an HGF, exhibits two topologically invariant properties – the number of Kekulé structures and Clar covers. The number of Kekulé structures K for a C_nH_m PAH is the number of conceivable arrangements of $n/2$ localized π bonds in a given structure. The second invariant – the number of Clar covers – is less frequently used and requires some explanation. A Clar cover of order k is a feasible resonance structure obtained by arranging k aromatic Clar sextets and $(n/2 - 3k)$ localized π bonds in a given structure. The maximal number of aromatic Clar sextets that can be accommodated in a given benzenoid structure is usually referred to as the Clar number Cl. The number of Clar covers C is defined as the total number of Clar covers of order k with k between 0 and Cl. The connection between the number of Kekulé structures and the π-conjugation strength is well-understood, as K defines the number of many-electron basis function in the configuration interaction (CI) expansion of the π energy. It is noted here that the present CI expansion consists only of covalent, non-ionic electronic states. It is clear that enlarging the CI space leads to lower energy. Analogously, producing a single epoxide-type site in a graphene flake reduces the number of Kekulé structures for a given flake and consequently will lead to an increase in the π energy. Using the number of Kekulé structures for quantifying the degree of π-conjugation has a single disadvantage: it implicitly assumes that all basis functions contribute to the lowest-energy CI wave function to a similar degree. It is possible to correct for this oversimplified picture by introducing multiple-counting for structures, in which favorable local arrangement of localized π bonds can be described as an aromatic Clar sextet. Obviously, these basis functions will have larger contribution to the CI energy than other basis functions with unfavorable local arrangements of the localized π bonds. Such a correction can be achieved if one counts C instead of K. Both topological invariants K and C are computed with the use of an automatic computer code developed for calculation of the Zhang–Zhang (ZZ) combinatorial polynomial;[32–34] K is given as the free-term coefficient of the ZZ polynomial and C is computed as a sum of all coefficients of the ZZ polynomial. The number of Kekulé

structures K and the number of Clar covers C can grow very fast with the number of atoms. For the largest HGF considered here, $C_{312}H_{48}$, K is larger than 10^{21} and C is larger than 10^{28}, which prevented the computation of C for the epoxidized isomers of this structure. Consequently, Table S1 in ESI† and Fig. 3 list only the results obtained with the number of Kekulé structures for this graphene flake.

Results and discussion

Quantum chemical descriptions of graphene oxidation

We begin with an analysis of structure **1** (phenanthrene). The DFT and DFTB energies associated with oxygen addition at bonds α–η are shown in Fig. 2(a). We briefly note here that DFTB and DFT are generally in good agreement with respect to optimized geometries of these HGFs (Fig. S1, ESI†). This agreement is consistent with previous investigations of functionalized carbon nanosystems.[29,35] The oxidation of phenanthrene to yield phenanthrene monoxide (denoted **1o**) can be understood in terms of two competing factors – the disruption of the π-conjugation and the geometrical deformation of the structure itself. The latter can even cause the cleavage of the C–C σ-bond such that an ether product becomes the optimized structure rather than an epoxy product.[26] This fact gives rise to a large discrepancy between optimized energies on the one hand, and the energy associated with disrupting π-conjugation alone on the other (the latter being determined using π-Hückel molecular orbital theory and Kekulé–Clar topological invariants, to be discussed in detail later). The most noticeable discrepancy in this regard corresponds to oxygen addition at the ι C–C bond (the bond fusing two hexagons). While its oxidation is the least energetically favorable according to DFT and DFTB, it is the third most optimal position at which π-conjugation may be disrupted. The opposite is the case for oxidation at the η C–C bond that corresponds to the most localized π-bond in the system, which is consequently attacked first in halogen addition reactions. Epoxidation of this bond leads to the largest disruption of π-conjugation, yet DFT/DFTB ΔE are the third largest. It is clear therefore that it is not only the disruption of π-conjugation that results in the largest ΔE for the oxidation of this model HGF.

This issue has been elucidated further by a simplified energy decomposition analysis (EDA)[36] using DFTB. Fig. 2(b) and (c) detail this analysis for oxidation of **1** at the α and η C–C bonds, respectively. For this analysis, we define (relative to the combined energy of $O(^3P)$ and the pristine HGF) ΔE to be the optimized energy of the oxidized HGF; E_{def} (deformation energy) to be the energy of $O(^3P)$ and the HGF at the optimized geometry of the oxidized HGF separated by an infinite distance; and E_{int} (interaction energy, $\Delta E - E_{def}$) to be the net interaction energy between the deformed HGF and $O(^3P)$. The latter arises from the C–O–C bond formation (stabilization) as well as the disruption of π-conjugation (destabilization). In the case of oxidation at the α C–C bond of **1o**, Fig. 2(b) shows that the interaction energy overwhelms the deformation energy, which results in the breaking of the α C–C σ-bond and the bending of the conjugated structure. For oxidation at the η C–C bond (Fig. 2(c)), we see the opposite trend to that of the α C–C bond. In this case, the most energetically favorable structure is an approximately planar one, with the η C–C σ-bond remaining intact. Symmetrical 'buckling' of this structure about its C_2 axis (forming a C–O–C moiety, but breaking the η C–C σ-bond) results in a structure *ca.* 150 kJ mol^{-1} higher in energy. Comparison of Fig. 2(b) and (c) shows that E_{def} for both α and η positions is approximately the same. On the other hand, E_{int} for the α isomer is greater compared to that of the η isomer. This is because the cleavage of the α C–C σ-bond and the formation of the ether group allows the two affected aromatic rings to retain their π-conjugation. Thus, disruption of π-conjugation in the η isomer is the dominant factor determining its planar equilibrium geometry, since in this case no additional stabilization can be gained by the cleavage of the η C–C σ-bond. These observations are related to those made previously regarding the *exo*-functionalization of single-walled carbon nanotubes (SWCNTs).[35,37] In the latter case, the balance between the breaking of the C–C σ-bond and the perturbation of the π-conjugation or the CNT (by the adduct) largely governed whether the oxidized-SWCNT minimum energy structure exhibited an ether (disrupted C–C σ-bond) or epoxide (intact C–C σ-bond) functional group.

We now turn to the oxidation of the larger **2–5** and **7–11** HGF species. Quantum chemical and topological descriptions of the oxidation of these species are compared in Fig. 3. ΔE for singlet and triplet state structures **2o–5o** and **7o–11o** are given in Fig. S3 and S4 (ESI†), respectively. Due to the differing physical (edge) and electronic (π-conjugation) structures of HGFs **1–11**, this analysis should furnish a comprehensive understanding of the factors influencing epoxidation. In general terms, Fig. 3 shows that the reactivity of the closed-shell singlet state HGF towards oxidation increases near the HGF edge, as one may expect. It is typically the edge region that sees ether formation as a result of oxidation, as opposed to epoxidation (which dominates near the center of the HGF). Fig. 3 also shows however that less aromatic C–C bonds (such as position 16 in structure **4**) are also amenable to ether formation, despite not being at the HGF edge. However, this applies only to the closed-shell singlet state HGF oxides; triplet state species **1o–11o** always led to the formation of epoxide functional groups. Comparison of Fig. 3 and Fig. S2 (ESI†) shows that ΔE near the edge of the HGF structure is defined by the interplay of the physical and electronic structures of the HGFs. For both the zigzag-edged **2o–4o** and the armchair-edged **5o**, **7o** and **8o**, this leads to ΔE being extremely fluxional between *ca.* −200 and −350 kJ mol^{-1} in this region. We discuss the case of structure **4** to illustrate this point: Fig. S2 (ESI†) shows that oxidation at positions 29, 26 and 27 yields ΔE values of −254, −303 and −237 kJ mol^{-1}. Each of these adjacent positions resides on the HGF edge (Fig. 1 and 3). The extreme deviation in ΔE, some 60–70 kJ mol^{-1}, correlates with the aromaticity of each respective C–C bond. In this case, positions 27 and 29 both belong to aromatic sextets, this stronger π-bonding leads to a weaker interaction with the functionalizing oxygen atom. This point is further illustrated by comparing these positions with their analogues (40, 36 and 37) in structure **9**. Fig. S2 (ESI†)

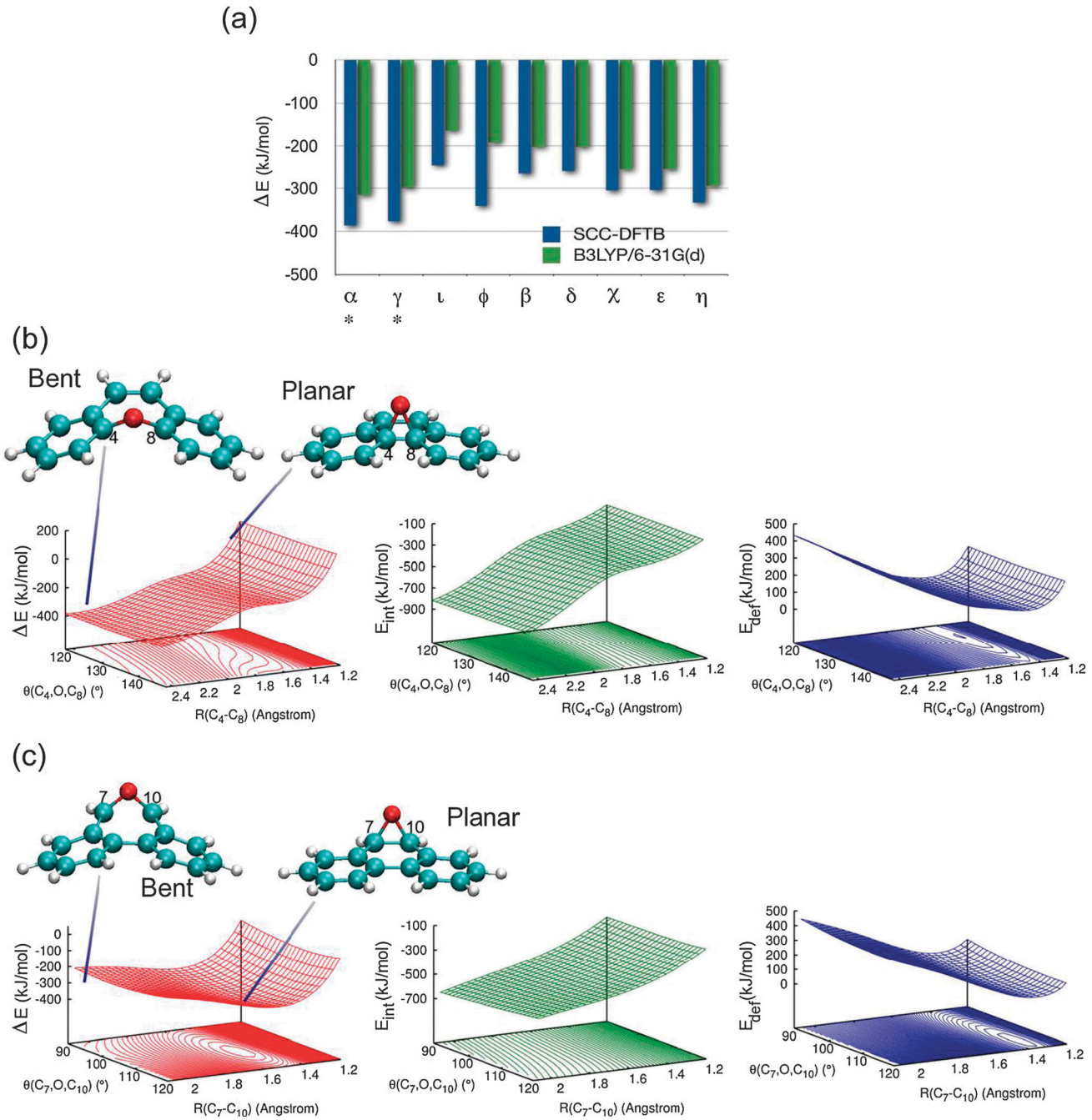

Fig. 2 (a) Relative energies of **1o** as a function of oxygen position using DFTB and DFT methods. Horizontal axis labels are ordered in terms of increasing Hückel energy; asterisks denote those positions at which oxidation leads to ether formation. ΔE (red), E_{int} (green) and E_{def} (blue) for O addition at (b) α and (c) η positions show the effects of conjugation disruption and structural deformation on the total DFTB energy. Energy contours are spaced at intervals of 10 kJ mol^{-1}.

shows that ΔE are −218, −188 and −223 kJ mol^{-1}, respectively. Each of these positions belongs to an aromatic sextet, oxidation therefore yields more consistent reactivities relative to each other.

Near the center of these HGFs, the case is somewhat different; ΔE is determined essentially by the π-conjugation patterns of each individual HGF, as is also the case for the archetypal species **6**. For example, ΔE at α, β, χ and δ positions of **6o** (Fig. 3) are −168, −190, −280 and −296 kJ mol^{-1}. The saw-toothed pattern observed in Fig. S2 (ESI†) for structures **2o–4o** is also evident for structure **5o**; the π-conjugation of each of these structures features isolated Clar-sextets as shown in Fig. 1. Structure **5** is in this respect an interesting case, in that it features a zigzag edge structure, yet also exhibits isolated Clar-sextet π-structure. For the zigzag-edged **5**, **7** and **8**, the π-conjugation structure is such that the most extremal oxidation positions (21, 14 and 30, respectively) are C=C double bonds. Consequently, oxidation at these positions leads to significantly increased ΔE. We note finally that these sawtooth patterns in ΔE discussed here

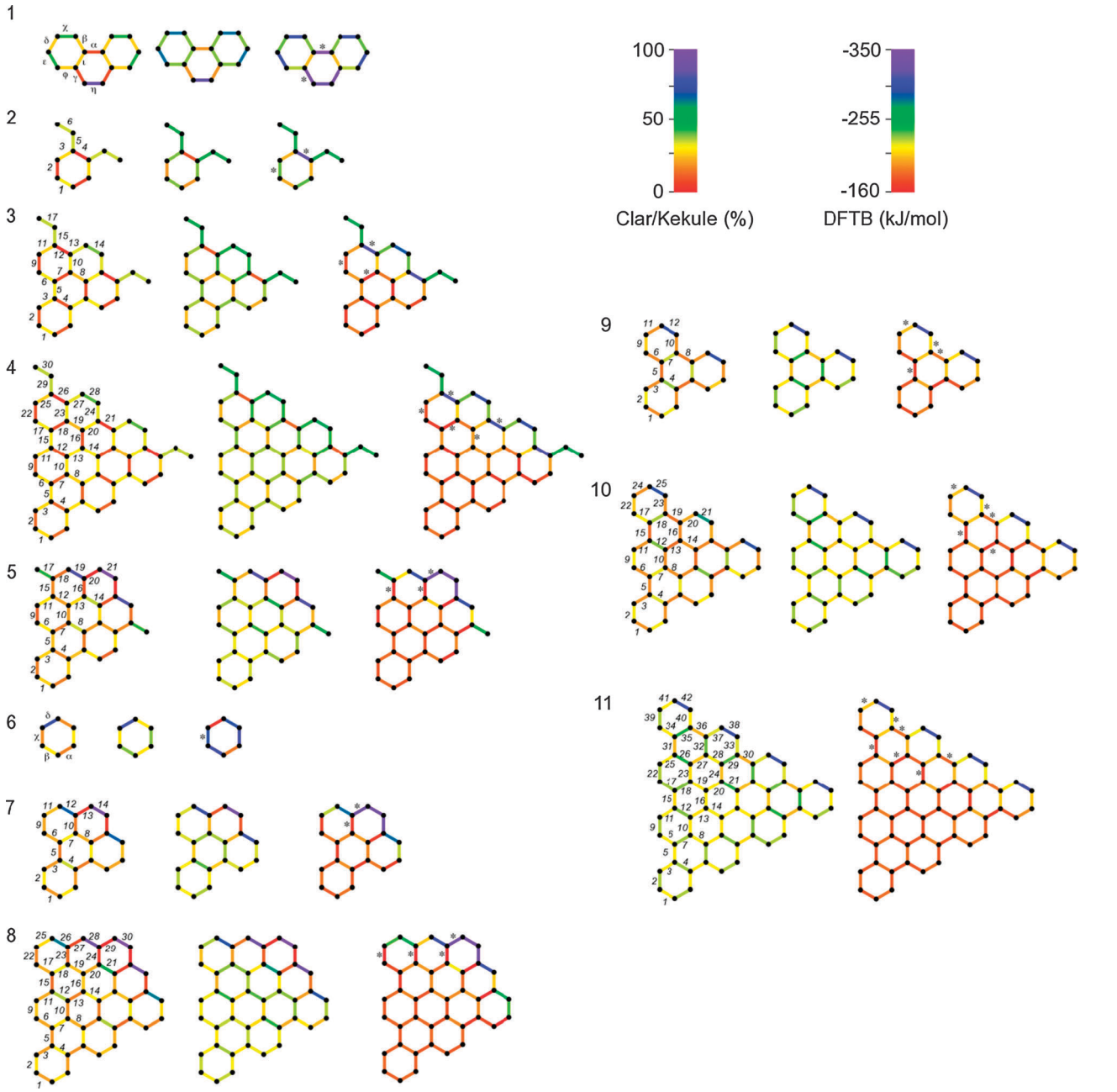

Fig. 3 Comparison of Clar (left), Kekulé (middle) and DFTB (right) descriptions of oxidation of HGFs **1–11**. Bonds are color-coded according to the % of conjugation remaining in the structure (Clar–Kekulé) or ΔE (DFTB); DFTB data correspond to singlet-state HGF oxides. Asterisks on DFTB structures denote those positions at which oxidation leads to ether formation. No triplet-state HGF oxide **1o–11o** featured ether formation, for any oxygen position (*i.e.* oxidation at all positions resulted in epoxide formation). ΔE values for all structures are provided in Fig. S3 and S4 (ESI†).

appear to manifest themselves more strongly in the smaller HGFs for each series. Thus, a size-effect regarding the impact of aromaticity on oxidation of these HGFs is evident, as is the increasing graphitic nature of the larger HGFs. A size effect is also evident in ΔE for the triplet state HGF oxides (Fig. S3, ESI†). Regarding the relative energetics of these closed-shell singlet and triplet HGF oxides, the singlet state is the lowest in energy according to SDFTB. This comparison also shows that oxidation of the closed-shell singlet ground state HGFs is more favourable in comparison to that of the triplet state HGFs. A size-effect on the singlet–triplet energy gap of HGFs is also evident in this comparison, since ΔE for the triplet HGF epoxides increase monotonically with increasing HGF size (Fig. 4). These trends are unsurprising, since it has been established that the relative energetics of singlet and triplet graphene nanoflakes, using density functional approaches, correlate directly with the amount of Hartree–Fock exchange correlation included in the description of electronic structure (DFTB being based upon PBE[38,39]). In essence, a higher degree of HF exchange leads to a decrease in the singlet–triplet energy gap.

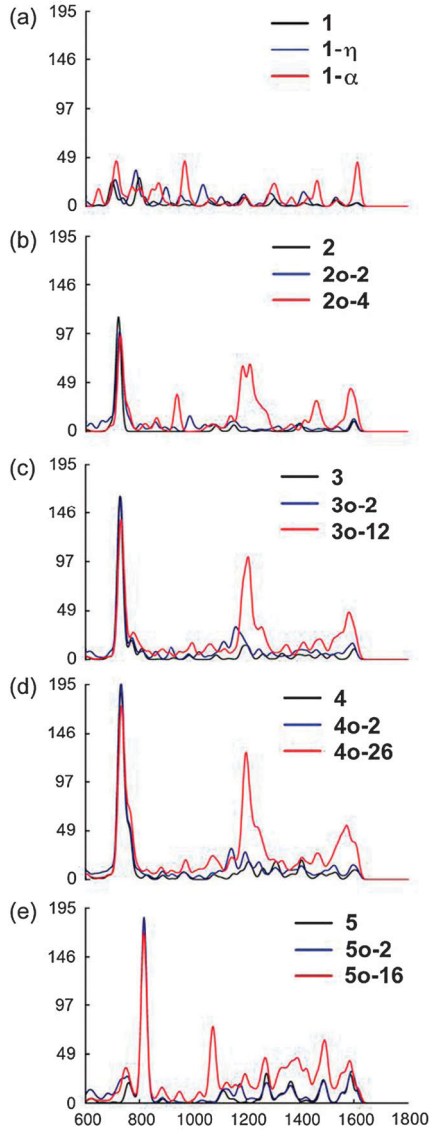

Fig. 4 (a)–(e) IR spectra of isolated Clar-sextet species **1–5** and **1o–5o** between 600 and 1800 cm^{-1}. The IR spectra of species with oxygen near the edge and center of the HGF are depicted in red and blue, respectively. Spectra in black are those of the respective pristine HGFs. Position numbers are defined in Fig. 1. Peak intensities (vertical axis) given in km mol^{-1} and vibrational wavenumbers (horizontal axis) given in cm^{-1}.

We note finally that no instances of sudden spin polarization in either pristine or oxidized species **1–11** were observed here using SDFTB, even after starting self-consistency cycles from broken symmetry spin densities as initial guess. This may not be the case for larger flakes, in which higher spin states (as well as broken spin-symmetry states in the case of zigzag edge HGFs) become energetically competitive.

As was the case for species **1**, large discrepancies between ΔE and the predictions of Hückel theory are also observed for the larger HGFs **2–5** and **7–11**. The same interplay between the disruption of π-conjugation and the structural deformation that was observed for **1o**, discussed above, is also observed for **2o–5o** and **7o–11o**. This analogy between the latter model system and the larger HGFs may also be extended to the EDA presented above for the case of **9o** (see Fig. S4, ESI†). It is noted here that these bonding trends are effectively the same as those observed by Zheng *et al.*,[35,37] who investigated the endo- and exohedral oxidation of SWCNTs, and Addicoat *et al.*,[29] who investigated hydrogenated and hydroxylated fullerenes. Thus, the factors governing the functionalization of graphene, SWCNTs and fullerenes may seemingly be understood in a common language.

Topological descriptions of graphene oxidation

We turn now to consider descriptions of graphene oxidation obtained using topological models of π-conjugation, *viz.* the Kekulé–Clar invariants. The calculated degrees of π-conjugation in epoxidized HGFs **1o–11o**, computed with the use of both Kekulé and Clar invariants, are given in Fig. 3 and Table S1 (ESI†). The extent to which the number of resonant structures in an epoxidated HGF is reduced depends on the position of the epoxide group. Interestingly, the largest and smallest disruptions are observed near the HGF edge. Epoxidation near the interior of the HGF, on the other hand, results in more homogeneous disruption of π-conjugation. This is particularly the case for the largest HGF structures here, as one may expect. At the HGF edge, epoxidation is most favourable at those positions exhibiting localized C=C double bonds; we note here that epoxidation at such sites causes little disruption of the π-conjugation of the HGF as a whole. This is illustrated by structure **8o**, for which epoxidation at position 30 (a C=C double bond) results in the disruption of 3% of the π-conjugation of the entire structure. Conversely, epoxidation at the adjacent position 29 results in the catastrophic destruction of 98% of the HGF's π-conjugation. These results suggest that epoxidation of finite graphenes will occur most probably in the vicinities of graphene edges, dislocations and defects. That is, those sites at which the disruption of localized C=C double bonds does not disrupt the large-scale electronic structure of the graphene.

At this point it is interesting to consider the correlation between quantum chemical and topological descriptions of HGF epoxidation. This comparison is made in Fig. S5 (ESI†), from which several observations can be readily made:

(1) For small structures (*e.g.* **1**, **2**, and **6**), there is no clear correlation between quantum chemical and topological data, suggesting that graph-theoretical approaches are applicable only in the case of large sp^2 structures. That is, the topological models of π-conjugation employed here are most useful in cases where quantum chemical investigation becomes prohibitively expensive.

(2) This correlation is best for un-optimized HGF epoxidated structures (*i.e.* those resembling pristine HGFs). Optimization of the geometry of the oxidized HGF invariably results in a lower energy structure, which cannot be reflected in the corresponding topological invariants. Thus, while the disruption of the π-conjugation is an important factor in predicting the preferred oxidation site for a particular finite graphene, it is by no means the sole factor.

(3) Aromaticities computed using the number of Kekulé structures are more accurate by *ca.* 20–30% compared to those computed using the number of Clar covers (with respect to DFTB energies of un-optimized epoxidized HGF structures).

Simulated IR spectra and correlation with experiment

Trends in ΔE for HGFs **1–11** discussed above are also reflected in their respective IR spectra. This is evident from Fig. 4, where the IR spectra of pristine HGFs **1–5** and their oxidized analogues **1o–5o** are compared. For each oxidized HGF we have considered epoxidation at electronically equivalent C–C bonds near the center (position 2) and near the edge (positions 4, 12, 26 and 16 for **2**, **3**, **4** and **5**, respectively) of each HGF structure. An extended comparison of DFTB and DFT IR spectra for species **1** is presented in ESI.†

For each HGF, the most intense IR peak in the region shown (Fig. 4 and 5) occurs between 700 and 800 cm^{-1}, which arises from the vibration of the HGF structure itself (not the C–O–C functional group). The effect of increasing HGF size on the intensity of this peak is clearly evident in Fig. 4a–e. The same may be said for the zigzag-edged series **6–8** (Fig. 5a–c), reflecting once again the increasing graphitic nature of the HGF with HGF size. Interestingly, this size effect is less obvious for species **9–11**, due to the decreased intensities exhibited by these species (Fig. 5d–f). While the spectra of species **1–5** between 1000 and 1600 cm^{-1} (Fig. 4) consist generally of distinct peaks – particularly for the smaller species – IR spectra of species **6–11** are more continuous in this region. This difference is ascribed to the differing aromaticities of, for example, positions 2 and 4 in species **2** (Fig. 4b) and positions 1 and 8 in species **7** (the latter being aromatic, while the former are not). Such an argument also explains the increasing difference between IR spectra of **1–5** and **6–11** with decreasing HGF size (where the C–C bond aromaticity becomes more dominant).

The IR spectra presented in Fig. 4 and 5 bear close resemblance to previously reported theoretical[40] and experimental[17,18,41,42] GO IR spectra. Epoxidation of **1–11** near the edge of the HGF structure yields two intense bands at *ca.* 1000–1200 (C–O–C bending/asymmetric stretch) and 1500–1600 cm^{-1} (C–C/C–O–C stretch). The prominent peak near 1200 cm^{-1} is consistent with the experimental results of Acik *et al.*,[17] who attributed this peak to the asymmetric vibration of C–O–C groups near *defect* sites at the graphene edge (as do Fuente *et al.*[40]). Acik *et al.* note, however, that upon aggregation of so-called 'edge-ethers' this peak is red-shifted to *ca.* 800 cm^{-1}. Nevertheless, this peak is observed here both in the presence of only a single C–O–C group (admittedly without the enhanced intensity found for aggregated epoxidized structures), and in the *absence* of edge defects (*i.e.* the graphene edge here is pristine). Furthermore, this spectral feature is in fact an intrinsic property of the GO *edge*; Fig. 4 and 5 show that the formation of epoxides near the center of the HGF decreases the intensity of this peak significantly.

The intensity of these peaks between 1000 and 1200 cm^{-1} is essentially the result of the C–C σ-bond being cleaved following oxygen addition (forming an ether), and corresponds to an increased ΔE at these positions (see Fig. 2). These peaks are much less intense, if not entirely absent, in the case of epoxidation at

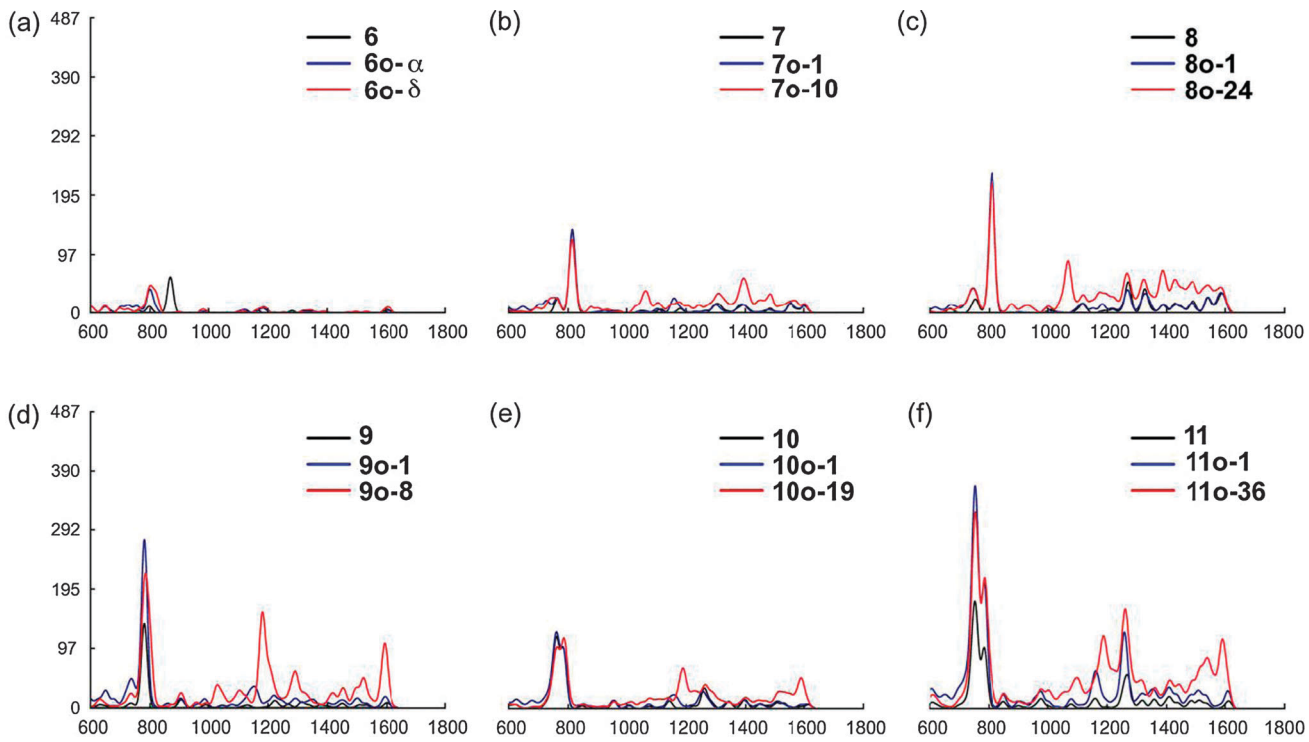

Fig. 5 (a)–(f) IR spectra of resonant Clar-sextet species **6–11** and **6o–11o** between 600 and 1800 cm^{-1}. The IR spectra of species with oxygen near the edge and center of the HGF are depicted in red and blue, respectively. Spectra in black are those of the respective pristine HGFs. Position numbers are defined in Fig. 1. Peak intensities (vertical axis) given in km mol^{-1} and vibrational wavenumbers (horizontal axis) given in cm^{-1}.

position 2 of species **1o–11o**. It is these positions at which the C–C σ-bond remains intact following epoxidation, resulting in a lower ΔE. These IR spectral signatures therefore serve as a convenient indicator of GO structure; the existence of ethers *versus* epoxides can be deduced from IR spectra alone. This is consistent with recent experimental work concerning the thermal reduction of GO. Bagri *et al.*[18] reported that thermal annealing of GO at 448 K results in the removal of peaks assigned to epoxides, thus indicating epoxide loss at this temperature. Such epoxide loss due to high-temperature thermal annealing has indeed been reported on a number of occasions.[8,17,18,41] However, upon annealing at even higher temperatures (1023 K), Bagri *et al.* observed that peaks assigned to ethers in the GO basal plane persisted in the IR spectrum. Such persistence of ether peaks in experimental GO IR spectra at high temperature points directly to the relative thermodynamic stabilities of ethers *versus* those of epoxides, and thus correlates exactly with the trends in ΔE and IR spectral intensities reported here. Presumably C–C σ-bond cleavage at high temperatures is driven by the increased thermal energy available. Nevertheless, Larciprete *et al.*[8] contend that ethers may also form *via* the oxidation of graphene defect sites; X-ray photoelectron spectroscopy measurements also show that such 'defect' GO ether groups exhibit higher stability at lower oxygen coverage.

Simulated Raman spectra and correlation with experiment

Raman spectra of **1–11** and **1o–11o** computed using DFTB are shown in Fig. 6 and 7. The Raman spectra for these pristine HGFs between 1000 and 2000 cm^{-1} are dominated by the D and G bands near 1300 and 1600 cm^{-1}, respectively, as one would expect. In the case of **3**, **6** and **7**, the relative intensities of these two bands are consistent with previous experimental[43,44] and theoretical data;[45,46] the greater intensity of the D band here has both structural and electronic origins.[45] We also note that Raman spectra of pristine/epoxidized graphene and CNTs share a general commonality, *viz.* a notable decrease in Raman peak intensities following oxidation for both ether and epoxide.[47] This is perhaps not unexpected, since the reduction in Raman peak intensities in the latter case is driven by the CNT structural deformation (and hence loss of symmetry) due to oxidation, as is observed in this work for GO. However, in the case of GO Fig. 6 and 7 show that the largest reduction in Raman activity occurs in or near the D band, with the G band remaining largely unchanged. On the other hand, Irle *et al.*[47] reported that the intensities of both the D and G bands were reduced following oxidation in the case of CNTs.

This reduction in D band intensity is coupled with a general broadening of the band itself. Previous experiments[42,48] have attributed this broadening near 1300 cm^{-1} to the formation of defects in the graphene structure as a result of oxidation. However, we can assign this broadening to the introduction of new peaks corresponding to symmetric C–O stretch modes, since our GO models are structurally pristine. Such broadening in this region can therefore be considered to be a signature of graphene oxidation itself, and not merely a signature of the introduction of defects into the graphene structure.

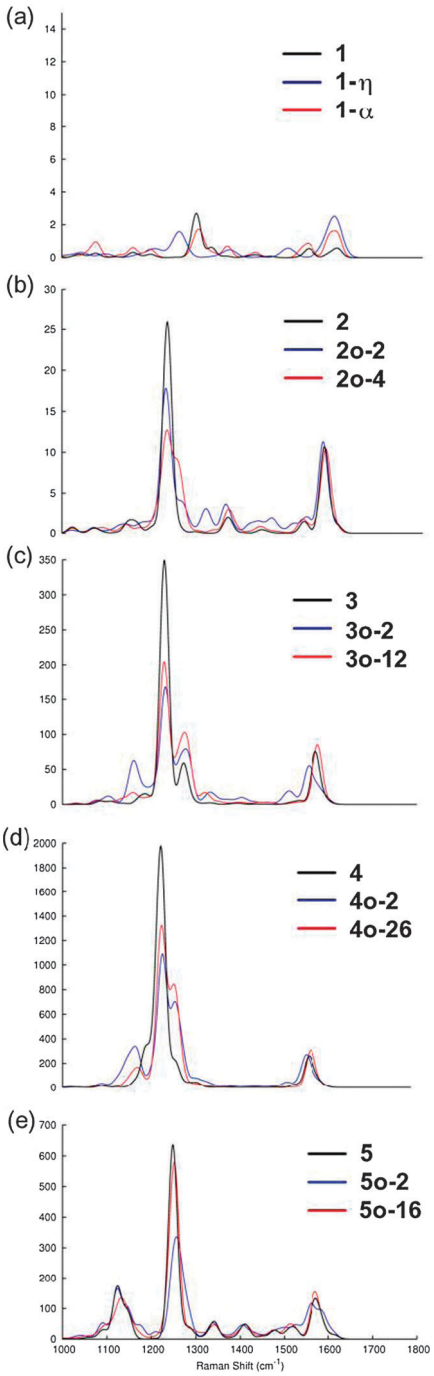

Fig. 6 (a)–(e) Raman spectra of isolated Clar-sextet species **1–5** and **1o–5o** between 600 and 1800 cm^{-1}. The spectra of species with oxygen near the edge and center of the HGF are depicted in red and blue, respectively. Spectra in black are those of the respective pristine HGFs. Position numbers are defined in Fig. 1. Activities (vertical axis) given in a.u. and vibrational wavenumbers (horizontal axis) given in cm^{-1}.

Fig. 6 and 7 show that Raman spectroscopy is a useful tool to delineate pristine graphene structures from their oxidized counterparts. Keeping in mind that the GO models employed here include only a single oxygen atom, one may realistically expect these two hallmarks of graphene oxidation (*i.e.* reduction in peak intensity and broadening near 1300 cm^{-1}) to be more extensive in an

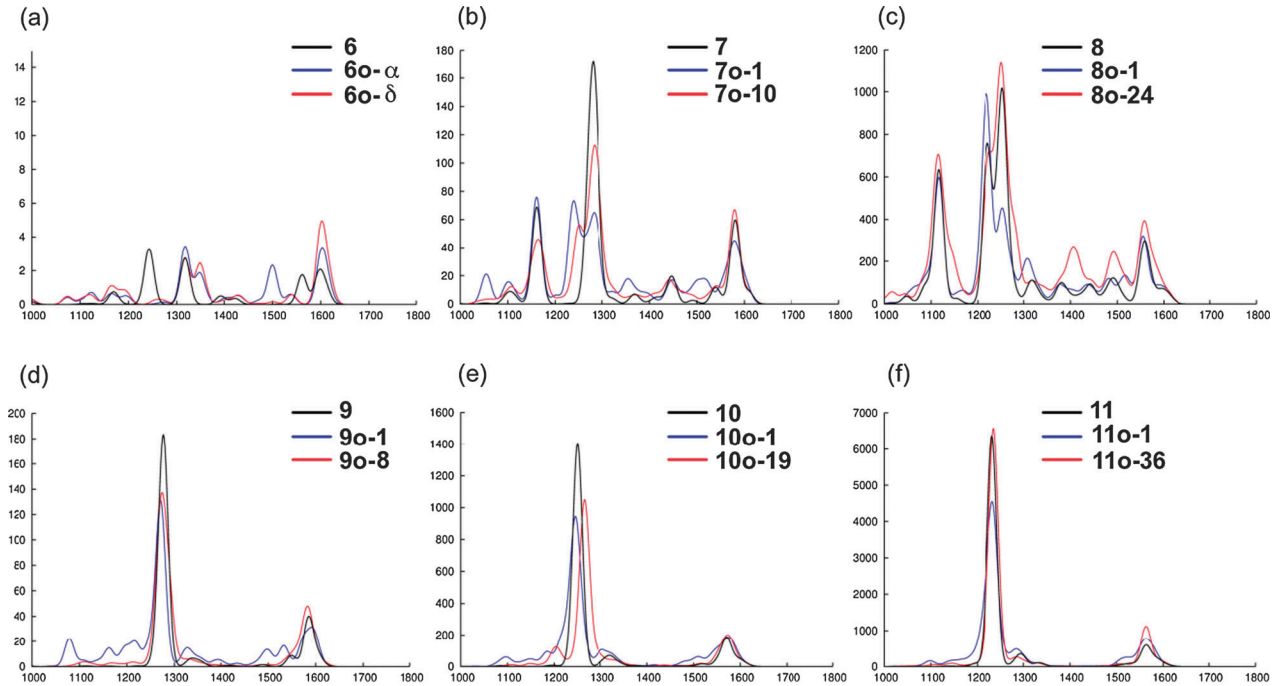

Fig. 7 (a)–(f) Raman spectra of resonant Clar-sextet species **6–11** and **6o–11o** between 600 and 1800 cm^{-1}. The spectra of species with oxygen near the edge and center of the HGF are depicted in red and blue, respectively. Spectra in black are those of the respective pristine HGFs. Position numbers are defined in Fig. 1. Activities (vertical axis) given in a.u. and vibrational wavenumbers (horizontal axis) given in cm^{-1}.

experimental situation. However, the relationship between thermodynamic stability and Raman spectroscopy is less noticeable compared to that for IR spectroscopy, if at all. That is, Fig. 6 and 7 do not assist in identifying the nature of the oxidation (*i.e.* ether *versus* epoxide in this case) as do Fig. 4 and 5. In this sense, therefore, IR spectroscopy is a more useful indicator of GO structure.

Conclusions

We have presented a detailed analysis of the nature of the epoxide and ether functional groups in model graphene oxide systems and their relationship with IR/Raman spectra. In each system, the relative thermodynamic stabilities of the oxide isomers were governed by two competing factors – *viz.* the disruption of the graphene structure's π-conjugation and the geometrical deformation of the structure itself. The most thermodynamically favorable oxidation positions resulted from the simultaneous minimization of the former, and the maximization of the latter, and were affected by the ability of the oxidized structure to maintain aromaticity *via* the cleavage of C–C σ-bonds. Computed IR spectra for each system also show that the IR spectral activity between *ca.* 600 and 1800 cm^{-1} correlated closely with these relative thermodynamic stabilities. In particular, the most thermodynamically stable GO isomers exhibited the most IR activity in this region, while the most thermodynamically unstable GO isomers exhibited relatively little IR activity by comparison. On the other hand, although GO can be told apart from an equivalent graphene *via* Raman spectroscopy, the correlation between Raman activity and thermodynamic stability of different GO structures was not observable. Finally, we note that when geometrical deformation was minimal, the Hückel method and graph-theory based topological invariants effectively predicted the results gained from density functional based methods, which are more computationally expensive by two or three orders of magnitude. We believe that this fact should remind the community of the physical insight that is made possible by the use of such conceptually simple techniques in the context of graphene/SWCNT functionalization.

Acknowledgements

This work was in part supported by a CREST (Core Research for Evolutional Science and Technology) grant in the Area of High Performance Computing for Multiscale and Multiphysics Phenomena from the Japanese Science and Technology Agency (JST). Computer simulations were performed using The Academic Center for Computing and Media Studies (ACCMS) at Kyoto University. A.J.P. acknowledges the Kyoto University Fukui Fellowship. B.Q.P. acknowledges the Japan–East Asia Network of Exchange for Students and Youth (JENESYS) program.

Notes and references

1 A. K. Geim and K. S. Novoselov, *Nat. Mater.*, 2007, **6**, 183–191.
2 S. Park and R. S. Ruoff, *Nat. Nanotechnol.*, 2009, **4**, 217–224.
3 D. R. Dreyer, S. Park, C. W. Bielawski and R. S. Ruoff, *Chem. Soc. Rev.*, 2010, **39**, 228–240.

4 K. P. Loh, Q. Bao, G. Eda and M. Chhowalla, *Nat. Chem.*, 2010, **2**, 1015–1024.
5 H. He, T. Riedl, A. Lerf and J. Klinowski, *J. Phys. Chem.*, 1996, **100**, 19954–19958.
6 A. Lerf, H. He, M. Forster and J. Klinowski, *J. Phys. Chem. B*, 1998, **102**, 4477–4482.
7 T. Szabó, O. Berkesi, P. Forgó, K. Josepovits, Y. Sanakis, D. Petridis and I. Dékány, *Chem. Mater.*, 2006, **18**, 2740–2749.
8 R. Larciprete, P. Lacovig, S. Gardonio, A. Baraldi and S. Lizzit, *J. Phys. Chem. C*, 2012, **116**, 9900–9908.
9 N. A. Vinogradov, K. Schulte, M. L. Ng, A. Mikkelsen, E. Lundgren, N. Mårtensson and A. B. Preobrajenski, *J. Phys. Chem. C*, 2011, **115**, 9568–9577.
10 J. T. Paci, T. Belytschko and G. C. Schatz, *J. Phys. Chem. C*, 2007, **111**, 18099–18111.
11 N. Lu, D. Yin, Z. Li and J. Yang, *J. Phys. Chem. C*, 2011, **115**, 11991–11995.
12 T. Sun and S. Fabris, *Nano Lett.*, 2011, **12**, 17–21.
13 P. M. Ajayan and B. I. Yakobson, *Nature*, 2006, **441**, 818.
14 X. Gao, L. Wang, Y. Ohtsuka, D.-E. Jiang, Y. Zhao, S. Nagase and Z. Chen, *J. Am. Chem. Soc.*, 2009, **131**, 9663.
15 L. Ma, J. Wang and F. Ding, *Angew. Chem., Int. Ed.*, 2012, **51**, 1161–1164.
16 L. Liu, L. Wang, J. Gao, J. Zhao, X. Gao and Z. Chen, *Carbon*, 2012, **50**, 1690–1698.
17 M. Acik, G. Lee, C. Mattevi, M. Chhowalla, K. Cho and Y. J. Chabal, *Nat. Mater.*, 2010, **9**, 840–845.
18 A. Bagri, C. Mattevi, M. Acik, Y. J. Chabal, M. Chhowalla and V. B. Shenoy, *Nat. Chem.*, 2010, **2**, 581–587.
19 A. D. Becke, *J. Chem. Phys.*, 1993, **98**, 5648–5652.
20 C. Lee, W. Yang and R. G. Parr, *Phys. Rev. B: Condens. Matter Mater. Phys.*, 1988, **37**, 785.
21 M. J. Frisch, G. W. Trucks, H. B. Schlegel, G. E. Scuseria, M. A. Robb, J. R. Cheeseman, G. Scalmani, V. Barone, B. Mennucci, G. A. Petersson, H. Nakatsuji, M. Caricato, X. Li, H. P. Hratchian, A. F. Izmaylov, J. Bloino, G. Zheng, J. L. Sonnenberg, M. Hada, M. Ehara, K. Toyota, R. Fukuda, J. Hasegawa, M. Ishida, T. Nakajima, Y. Honda, O. Kitao, H. Nakai, T. Vreven, J. J. A. Montgomery, J. E. Peralta, F. Ogliaro, M. Bearpark, J. J. Heyd, E. Brothers, K. N. Kudin, V. N. Staroverov, R. Kobayashi, J. Normand, K. Raghavachari, A. Rendell, J. C. Burant, S. S. Iyengar, J. Tomasi, M. Cossi, N. Rega, J. M. Millam, M. Klene, J. E. Knox, J. B. Cross, V. Bakken, C. Adamo, J. Jaramillo, R. Gomperts, R. E. Stratmann, O. Yazyev, A. J. Austin, R. Cammi, C. Pomelli, J. W. Ochterski, R. L. Martin, K. Morokuma, V. G. Zakrzewski, G. A. Voth, P. Salvador, J. J. Dannenberg, S. Dapprich, A. D. Daniels, Ö. Farkas, J. B. Foresman, J. V. Ortiz, J. Cioslowski and D. J. Fox, *Gaussian 09, Revision A.1*, Gaussian, Inc., Wallingford, CT, 2009.
22 M. Elstner, D. Porezag, G. Jungnickel, J. Elsner, M. Haugk, T. Frauenheim, S. Suhai and G. Seifert, *Phys. Rev. B: Condens. Matter Mater. Phys.*, 1998, **58**, 7260–7268.
23 C. Kohler, G. Seifert, U. Gerstmann, M. Elstner, H. Overhof and T. Frauenheim, *Phys. Chem. Chem. Phys.*, 2001, **3**, 5109–5114.
24 E. Malolepsza, H. A. Witek and K. Morokuma, *Chem. Phys. Lett.*, 2005, **412**, 237–243.
25 H. A. Witek, K. Morokuma and A. Stradomska, *J. Chem. Phys.*, 2004, **121**, 5171–5178.
26 W. Li, S. Irle and H. A. Witek, *ACS Nano*, 2010, **4**, 4475–4486.
27 H. A. Witek, S. Irle, G. Zheng, W. A. de Jong and K. Morokuma, *J. Chem. Phys.*, 2006, **125**, 214706–214715.
28 H. A. Witek, K. Morokuma and A. Stradomska, *J. Theor. Comput. Chem.*, 2005, **4**, 639–655.
29 M. A. Addicoat, A. J. Page, Z. E. Brain, L. Flack, K. Morokuma and S. Irle, *J. Chem. Theory Comput.*, 2012, **8**, 1841–1851.
30 D. Řeha, H. Valdés, J. Vondrášek, P. Hobza, A. Abu-Riziq, B. Crews and M. S. de Vries, *Chem.–Eur. J.*, 2005, **11**, 6803–6817.
31 D. Moran, F. Stahl, H. F. Bettinger, H. F. Schaefer and P. v. R. Schleyer, *J. Am. Chem. Soc.*, 2003, **125**, 6746–6752.
32 C. P. Chou and H. A. Witek, *MATCH*, 2012, **68**, 3–30.
33 C. P. Chou, Y. T. Li and H. A. Witek, *MATCH*, 2012, **68**, 31–64.
34 H. Zhang and F. Zhang, *Discrete Appl. Math.*, 1996, **69**, 147–167.
35 G. Zheng, Z. Wang, S. Irle and K. Morokuma, *J. Am. Chem. Soc.*, 2006, **128**, 15117–15126.
36 K. Morokuma and K. Kitaura, in *Chemical Applications of Electrostatic Potentials*, ed. P. Politzer and D. G. Truhlar, Plenum Press, New York, 1981, pp. 215–242.
37 Z. Wang, S. Irle, G. Zheng and K. Morokuma, *J. Phys. Chem. C*, 2008, **112**, 12697–12705.
38 J. P. Perdew, K. Burke and M. Ernzerhof, *Phys. Rev. Lett.*, 1996, **77**, 3865–3868.
39 J. P. Perdew, K. Burke and M. Ernzerhof, *Phys. Rev. Lett.*, 1997, **78**, 1396.
40 E. Fuente, J. A. Menéndez, M. A. Díez, D. Suárez and M. A. Montes-Morán, *J. Phys. Chem. B*, 2003, **107**, 6350–6359.
41 C.-M. Chen, Q. Zhang, M.-G. Yang, C.-H. Huang, Y.-G. Yang and M.-Z. Wang, *Carbon*, 2012, **50**, 3572–3584.
42 D. S. Sutar, P. K. Narayanam, G. Singh, V. D. Botcha, S. S. Talwar, R. S. Srinivasa and S. S. Major, *Thin Solid Films*, 2012, **520**, 5991–5996.
43 C. Mapelli, C. Castiglioni, E. Meroni and G. Zerbi, *J. Mol. Struct.*, 1999, **480–481**, 615–620.
44 C. Mapelli, C. Castiglioni, G. Zerbi and K. Müllen, *Phys. Rev. B: Condens. Matter Mater. Phys.*, 1999, **60**, 12710–12725.
45 F. Negri, C. Castiglioni, M. Tommasini and G. Zerbi, *J. Phys. Chem. A*, 2002, **106**, 3306–3317.
46 L. Wang, J. Zhao, Y.-Y. Sun and S. B. Zhang, *J. Chem. Phys.*, 2011, **135**, 184503.
47 S. Irle, A. Mews and K. Morokuma, *J. Phys. Chem. A*, 2002, **106**, 11973–11980.
48 T. Gokus, R. R. Nair, A. Bonetti, M. Böhmler, A. Lombardo, K. S. Novoselov, A. K. Geim, A. C. Ferrari and A. Hartschuh, *ACS Nano*, 2009, **3**, 3963–3968.